Soft Matter

Accepted Manuscript

This article can be cited before page numbers have been issued, to do this please use: A. Yousefi Siavoshani, Z. Fan and S. Wang, *Soft Matter*, 2026, DOI: 10.1039/D6SM00148C.

ROYAL SOCIETY OF CHEMISTRY

rsc.li/soft-matter-journal

View Article Online
DOI: 10.1039/D6SM00148C

How tip geometry controls fracture in ductile polymer glasses and brittle elastomers

Asal Y Siavoshani, Zehao Fan, and Shi-Qing Wang*
School of Polymer Science and Polymer Engineering, University of Akron, Akron, Ohio 44325

Abstract

Based spatially-temporally resolved polarized optical microscopic (*str*-POM) measurements we studied fracture behavior of ductile and brittle glassy polymers as well as highly crosslinked rubbers to draw the following conclusions: (1) There is no tip plasticity below a threshold load in ductile plastics such as polyethylene terephthalate. (2) In ductile polymer glasses, before tip yielding at a common tip stress the remote load scales with notch length a as $a^{-1/2}$, in agreement with the Inglis solution. (3) A finite stress saturation zone is observed in elastomers at loading levels even well below fatigue threshold due to significant crack tip blunting. (4) When thickness is small enough for the plane stress condition to prevail at crack tip, in double-edge notch tension (DENT) for both ductile glassy polymers and rubbers that is characterized by ligament length l, nominal strain in the ligament is defined by $\varepsilon_{lig} = X/l$, where X is tensile displacement; tensile force F increases linearly with X independent of l; tip stress increases linearly with the far-field σ_{lig} ($\sim \varepsilon_{lig}$). By demonstrating stress concentration at crack tip in DENT in elastic materials and characterizing crack propagation in ductile polymers, the present study fills the missing gap in our understanding of fracture behavior in a wider range of polymeric materials. The acquired knowledge may be useful to guide specific design for packaging materials.

* Corresponding author's email: swang@uakron.edu.

View Article Online
DOI: 10.1039/D6SM00148C

1. Introduction

After several decades of investigations on polymer fracture,[1-6] there has been significant progress to elucidate the origin of Griffith's scaling in brittle plastics[7, 8] and the hidden mechanisms controlling dynamic fracture of elastomers[9-11]. Specifically, applications of spatially and temporally resolved polarized light microscopic (*str*-POM) method, as a stress-based approach[12] to fracture mechanics of polymeric materials, have revealed how stress buildup at a notch tip as a function of remote load. The Inglis[13]-Creager-Paris[14]-solutions inspired approach has shown fresh insights[7, 8, 15, 16] into polymer fracture and led to the conclusion that lab-prepared notch in polymeric materials is not sharp and can be characterized with a finite "Inglis" radius. The existence of a sizable stress-saturation zone (SSZ) in polymeric materials[7] allowed the tip stress to be estimated. According to *str*-POM observations[7] brittle plastics show no evidence of tip yielding associated with emergence of plastic zone for PMMA at room temperature. Crack growth in elastomers reflects bond dissociation in backbones of load-bearing strands on a certain time scale;[9] high crack propagation speed requires high far-field stress not because of any higher viscoelastic energy dissipation but because only a higher degree of network stretching can shorten elastomer's lifetime, making the crack front advance faster. A recent re-visit[11] to delayed rupture[17] further elucidated the nature of elastomeric failure and established the phenomenological foundation.

There are still several outstanding topics in the field of polymer fracture. We address them in the present study by applying *str*-POM method for a range of polymeric materials, from ductile and brittle glassy polymers to elastomers. We confirm using ductile PET that no plastic zone forms at notch tip below a threshold load. This feature can be understood in terms of Inglis-Creager-Paris (ICP) solutions and reveals the non-Irwin nature of SSZ. Before tip yielding in ductile plastics, we verify the ICP description: the tip stress is proportional to the stress intensity factor $K = \sigma a^{1/2}$. In other words, remote load $\sigma \sim a^{-1/2}$ produces a common tip stress for different notch lengths. Our *str*-POM measurements further reveals existence of a finite (≥ 40 μm) stress saturation zone (SSZ) ahead the notch tip in a well crosslinked elastomer in a broad range of applied load both below the fatigue threshold and during crack growth, implying that even fatigue during cyclic load should involve high chain extension and scission on the length scale of SSZ well beyond a monolayer length scale. Additional *str*-POM observations demonstrate the stress field in double-edge-notch tension (DENT) in linear elastic limit and show for both plastics and elastomers that (a) ligament length l defines an effective strain $\varepsilon = X/l$ in terms of displacement X and (b) stress intensification at crack tip is linearly proportional to ε.

2. Materials and methods

2.1. Materials and Sample Preparation

The bisphenol-A polycarbonate (PC) and Polystyrene (PS) used in this study was sourced from Grainger and PS had thicknesses of B = 1.5 mm and 0.77 mm and PC had a thickness of 0.7 mm. The polyethylene terephthalate (PET) used in this study was obtained from Auriga Polymers and has a thickness of 0.2 mm.

View Article Online
DOI: 10.1039/D6SM00148C

Highly crosslinked butadiene rubber (BR) samples were prepared using 1 wt% dicumyl peroxide (DCP) as the curing agent. A 100 g batch of neat BR was first masticated on a two-roll mill for 30 min to ensure homogeneity. Subsequently, 1 wt% DCP was added to the matrix and thoroughly mixed. The resulting compound was then preheated at 140 °C for 5 min and compression-molded at 150 °C for 1 h to achieve fully isotropic crosslinked specimens with various thicknesses.

Single edge notches were primarily introduced into the ribbon shaped samples by gently hammering a razor into the edge, resulting in generation of a natural crack, akin to a method employed by Berry [18, 19], as done in the case of all PC and PET specimens.

Double-edge notch geometries were introduced into the ribbon-shaped specimens using a two-step process. First, a coarse notch was machined using a saw to remove the bulk of the material. This was subsequently sharpened into a natural crack by gently tapping a razor blade into the notch root; this method was employed to minimize plastic deformation and damage at the crack tip. Following preparation, the integrity of the crack tips was verified using cross-polarized light to detect any localized damage zones or residual stresses. If any such damage was observed, the specimens were annealed at a temperature near their glass transition temperature (Tg) to promote healing prior to mechanical testing.

2.2. Testing Instruments

Tensile tests were conducted using a universal testing machine (Instron 5969). The deformation process was recorded by a 4K camera (HY-6110 Micro Camera) equipped with an Arducam zoom lens (5–100 mm) to enable high-resolution video capture of the specimen during loading.

Entangled transparent polymers are known to exhibit stress-induced birefringence under deformation. The applied deformation generates anisotropy in the polymer network, leading to a change in birefringence Δn. To quantify this effect, photoelastic measurements were performed simultaneously with the tensile tests. Photoelasticity is an experimental technique that relates the optical response of a material (birefringence) to its internal stress state during deformation. In the present setup, polarizers were sourced from polarization.com and arranged in a standard transmission configuration. A sodium vapor lamp with wavelength $\lambda = 589$ nm was used as a monochromatic light source to illuminate the specimen. The transmitted light, after passing through the polarizer–specimen–analyzer assembly, was recorded by the 4K camera, allowing the evolution of stress-induced birefringence to be correlated with the mechanical response obtained from the tensile tests.

3. Experimental results

3.1 Griffith scaling in ductile glassy polymers in SEN

Whether amorphous polymers are ductile or brittle is often judged according to their macroscopic stress–strain response. Such a distinction, however, does not describe how failure is initiated in the presence of a crack. While ductile polymers can undergo plastic deformation under

View Article Online
DOI: 10.1039/D6SM00148C

sufficiently high loads, tip yielding can be avoided at low loads. In absence of plastic deformation at crack tip, we can examine whether ICP solutions are valid in the linear elasticity limit.

We apply the *str*-POM method to characterize the stress state at crack tip in the SEN configuration, specified by a notch of length a in a specimen of width W. As along as a/W < 0.2, stress intensity factor K shows negligible dependence[20] on W so that Griffith criterion to apply. The system under study is a polycarbonate with thickness B = 0.7 mm, which is sufficiently thin to avoid[8] being notch brittle. Figure 1a shows nominal stress vs. strain curves with a = 2, 4, 8, and 20 mm respectively. All specimens exhibit a ductile response, with the notch tip first reaching a yield point followed by localized necking without brittle failure.

Our str-POM measurements enable us to follow stress concentration at the notch tip in these four samples. For example, as shown in Fig. 1(b) at a common birefringence order of N_{tip} = 14 at the notch tip, just before the onset of tip yielding and plastic deformation, a finite zone (r_{ss} = 100 μm) of stress saturation (SSZ) is present. In other words, the stress building at the notch tip follows $r^{-1/2}$ scaling up to SSZ; the tip stress σ_{tip} depends on the far-field σ as $\sigma_{tip} \sim K = \sigma a^{1/2}$ so that $\sigma \sim a^{-1/2}$ produces a common tip stress, as shown in Fig. 1(c), which is consistent with Inglis solution[13] for an elliptical hole. The dependence of the peak nominal stress on a is much weaker, as shown by squares in Figure 1(c).

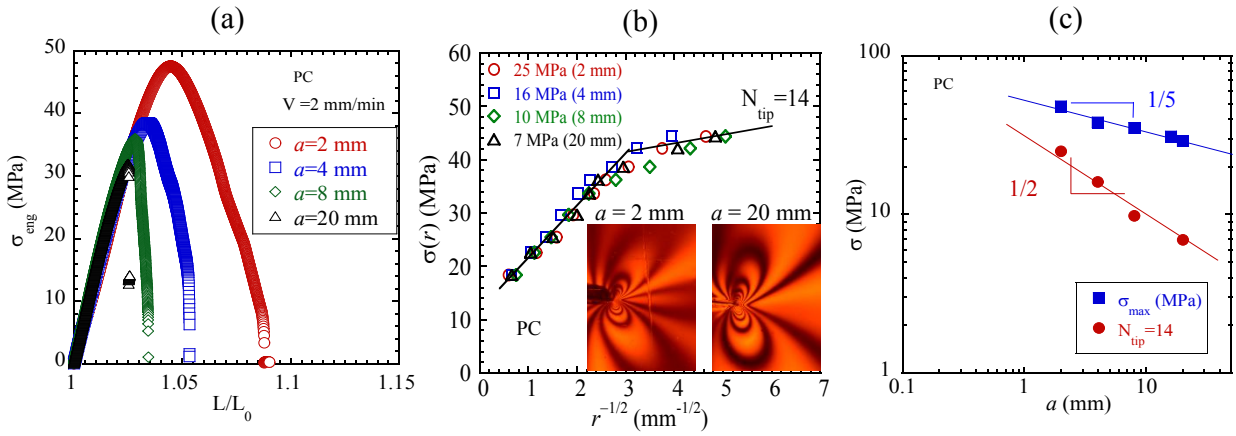

Figure 1 (a) Nominal stress–strain curves of PC SEN specimens with notch lengths a = 2 ,4, 8, and 20 mm, obtained at a crosshead speed V = 2 mm/min, where L_0 = 2W for each sample. (b) Local stress distribution ahead of the notch tip plotted against $r^{-1/2}$ at a common tip birefringence order N_{tip} = 14, involving different far field stress values (25, 16, 10, and 7 MPa), just prior to the onset of tip yielding, where the two images show the same birefringence order for two different notch sizes. (c) Nominal far-field stress σ at N_{tip} = 14 and at the peak remote load (maximum nominal stress in (a)) plotted against a.

We have demonstrated with ductile PC that it is only linear elastic before tip yielding. The sizable SSZ is not Irwin's plastic zone. According to the Creager-Paris solution,[14] the tip stress is

View Article Online
DOI: 10.1039/D6SM00148C

linearly proportional to the far-field load and below yield stress below a threshold load. We support this conclusion with a second ductile glassy polymer, i.e., polyethylene terephthalate (PET). Figure 2(a) contains three photos from *str*-POM observations, showing that there exists a wide range of far-field stress within which no tip yielding occurs. For example, Irwin-Dugdale plastic zone cannot be observed at and below $\sigma = 26$ MPa ($a = 2$ mm), as explained by the photos of identical birefringence patterns before and after application of $\sigma = 26$ MPa. There is no residual birefringence observed after unloading from $\sigma = 26$ MPa. On the other hand, we cannot rule out that plastic zone does not exist below the spatial resolution of our *str*-POM observation. Figure 2(b)-(d) are three equivalent plots, showing the near-tip stress field in terms of birefringence at 27 MPa for $a = 2$ mm, along with other three SEN samples that show the same fringe order of $N_{tip} = 25$ at the various levels of far-field stress and different notch lengths. We note that plateauing and converging features are exactly those encompassed by the Creager-Paris solution. Like PC, there exists a stress saturation zone, a bit larger than that of PC, ca. 160 μm. Each of the three Figures 2(b)-(d) indicates the same conclusion: the stress converges to a common value of 55 MPa.

Like PC, the far-field stress σ in PET required to produce this common tip stress scales linearly with $a^{-1/2}$, as shown in Figure 2(e). Moreover, the peak nominal stress scales with a in a weaker manner. In both Figure 1(a) and 2(a) the peak stress corresponds to the onset of stable ductile crack propagation.

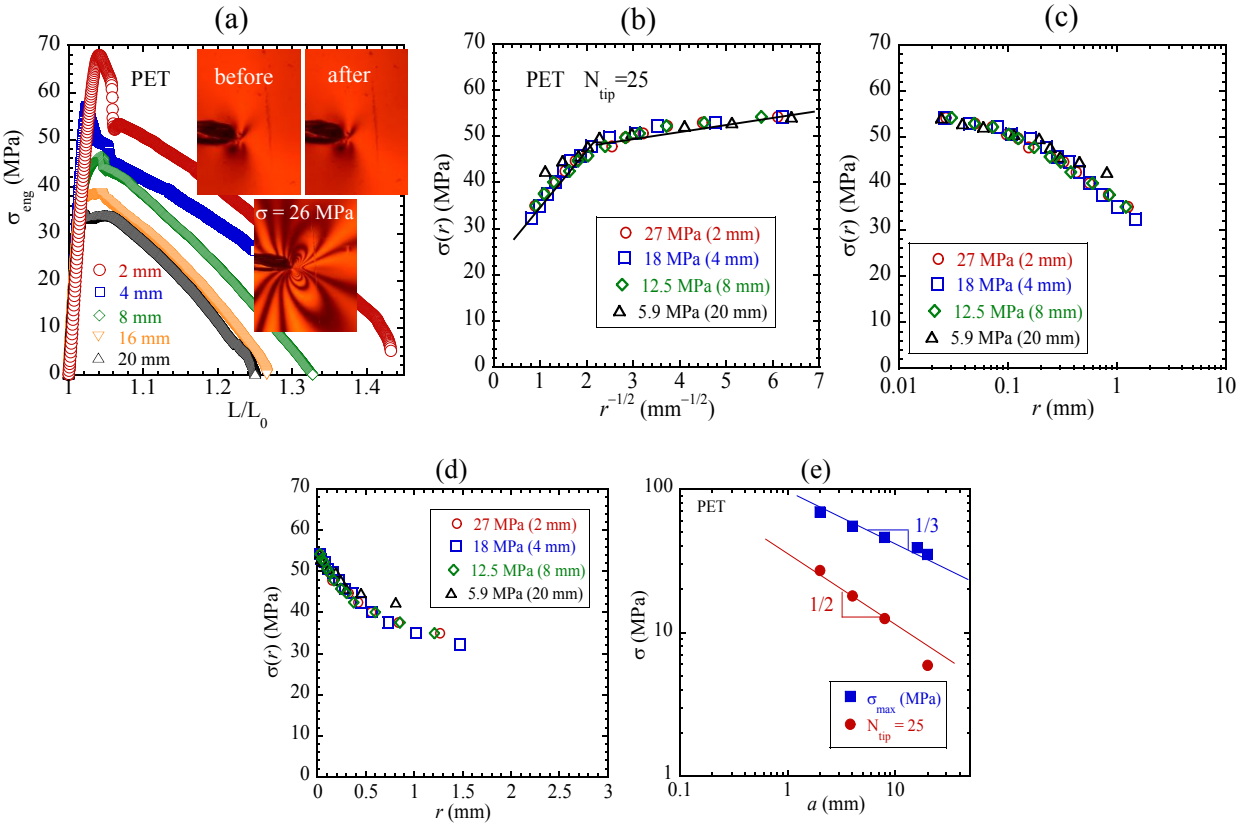

View Article Online
DOI: 10.1039/D6SM00148C

Figure 2 (a) Nominal stress–strain curves showing consistent ductile behavior in PET SEN specimens. The *str*-POM frames illustrate loading to $N_{tip} = 25$ and subsequent unloading back to the original tip pattern with no residual birefringence, indicating that the applied load is below the onset of tip yielding. (b)-(d) Local tip stress (from birefringence) plotted against $r^{-1/2}$ on linear and logarithmic scales, at a fixed tip stress corresponding to the isochromatic fringe order $N_{tip} = 25$, showing a finite stress-saturation zone in (b) and (c) and convergence to 55 MPa in (d). (e) Nominal far-field stress at $N_{tip} = 25$ and at the peak remote load (maximum nominal stress in (a)) plotted against $a^{-1/2}$.

3.2 Finite stress saturation zone in elastomers in SEN

Our *str*-POM observations[7, 8] including the present ones in Figures 1 and 2 indicate that crack tip in plastics are not sharp, leading to existence of a sizable stress saturation zone (SSZ) in SEN setting. Creager-Paris solution[14] explains that the origin of SSZ is the existence of a finite tip radius. More discussion is provided in Section 4 on the relationship between SSZ and the C-P solution.

A large SSZ[15] in prenotched elastomers also has implications. Using a highly-crosslinked polybutadiene, we apply *str*-POM method to quantify the stress intensification at notch tip. Stretching at V = 3 mm/min (L_0 = 30 mm) with cut size a = 3.4 mm produces stress response as shown in Figure 3(a) and allows us[16] to measure crack speed v_c on a continuous basis at various far-field loads. Figure 3(b) shows the existence of SSZ from σ = 0.03 to 0.12 MPa based on the birefringence images in Figure 3(c). The size of SSZ only increases with Figure 3(d) presents measured values of v_c at different values of σ in open circles above 0.1 MPa when crack growth becomes visible. See Movie SI.1 in Supporting Information. This disclosed relationship between v_c and σ permits us to indicate extrapolated values of v_c at 0.03, 0.05 and 0.07 MPa (e.g., 10^{-8} mm/s at 0.05 MPa) and to suggest that these loading levels are well below a fatigue threshold G_0. Typical cyclic loading usually produces crack growth much higher than 10^{-8} mm/s. At these loading levels a sizable SSZ is already present. At far-field stress equal to 0.12 MPa, crack growth is significant as shown in Figure 3d, with $r_{ss} \sim 110$ μm, implying that energy release involves a large scale far greater than monolayer scale. Since r_{ss} is also sizable well below fatigue threshold as shown in Figure 3b, cyclic crack growth during fatigue tests should also involve energy release on the length scale of r_{ss}. Our analysis suggested[10] that crack growth under applied load is due to chain network breakdown at crack tip via chain scission on time scale characterized by v_c and r_{ss}.

View Article Online
DOI: 10.1039/D6SM00148C

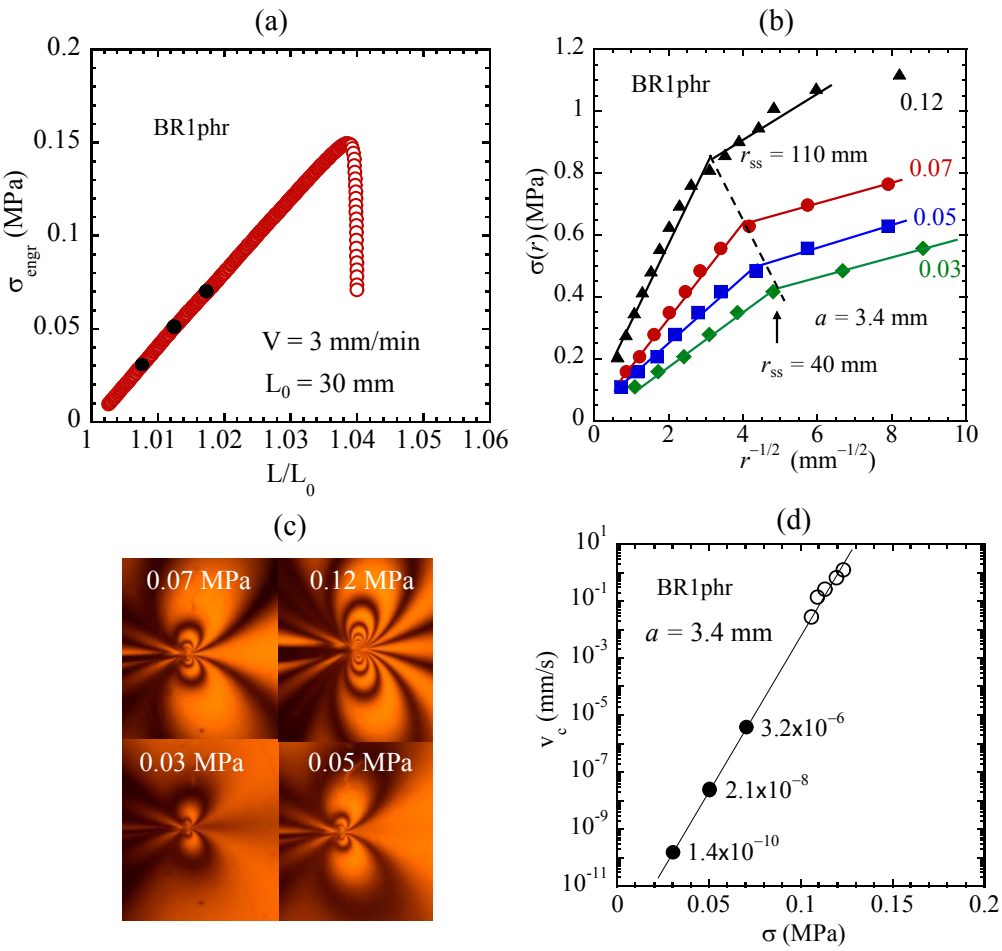

Figure 3 (a) Nominal stress vs. strain curve for BR1phr in SEN with length, width and thickness given by 30, 15 and 1.5 mm, and a = 3.4 mm, produced with V = 3 mm/min and L_0 = 30 mm. (b) Simultaneous s*tr*-POM measurements of local birefringence distribution with respect to the distance r to the at notch tip, plotted against $r^{-1/2}$ at four levels of far field loads: σ_0 = 0.03, 0.05, 0.07 and 0.12 MPa. (c) Four images at the four respective loads. (d) Crack speed v_c from video recording (Movie SI.1) of the same test described in (a)-(c), where three filled circles show the extrapolated values of v_c at 0.03, 0.05 and 0.07 MPa respectively, along with the actual reading of v_c in open circles.

3.3. Scaling behavior in terms of nominal and local stresses in DENT

While *str*-POM measurements[7-11] have been carried out to uncover physics in polymer fracture in SEN and pure shear, fracture in DENT configuration remains unexplored by *str*-POM method. Below, it is shown that *str*-POM measurements provide fresh insight into the nature of various scaling behavior uncovered by far-field measurements.

3.3.1 Effective strain

To investigate fracture characteristics of ductile polymers and discuss the framework of the essential work of fracture (EWF), we consider the DENT configuration. This geometry is

View Article Online
DOI: 10.1039/D6SM00148C

distinct from SEN typically used for brittle materials; it is designed to operate in the limit where the ligament length (l) is significantly smaller than the specimen width (D). In this regime ($l \ll D$), the ligament length becomes the sole characteristic length scale governing the deformation. Unlike geometries where fracture is dictated by crack length, the mechanical response of a ductile DENT specimen prior to global yielding or brittle fracture behaves analogously to a linear spring. In other words, we found the emergent tensile force to scale linearly with the applied displacement, effectively independent of l.

Unlike brittle polymers, in DENT of ductile glassy polymers, the tensile force also continues to increase beyond the point of tip yielding. Using a bisphenol-A polycarbonate (PC) sheet with thickness B = 0.77 mm and a polyethylene terephthalate (PET) sheet with B = 0.2 mm, Figs. 4(a)-(b) respectively illustrate that the tensile force F depends primarily on the displacement X in a linear fashion, independent of l up to the maximum force, at which point the entire ligament has undergone necking. Below we discuss the implications using dimensional analysis.

For F to depend on X but independent of l, we infer that the effective tensile stress σ_{lig} in the ligament must be higher in shorter ligaments at a common value of X. Specifically,

$$\sigma_{lig} = F/Bl = E_{lig}\varepsilon_{lig} \quad (1)$$

defines an the effective strain ε_{lig} is given by

$$\varepsilon_{lig} = X/l, \quad (2)$$

so that we have

$$F = (E_{lig}B)X. \quad (3)$$

Here the slope given by $E_{lig}B$ can be read from Figure 4(a)-(b) to reveal an effective modulus E_{lig}. We find E_{lig} = 0.43 GPa for PC, which is approximately four times smaller than the bulk Young's modulus E = 1.8 GPa. Similarly, E_{lig} = 0.75 GPa for PET.

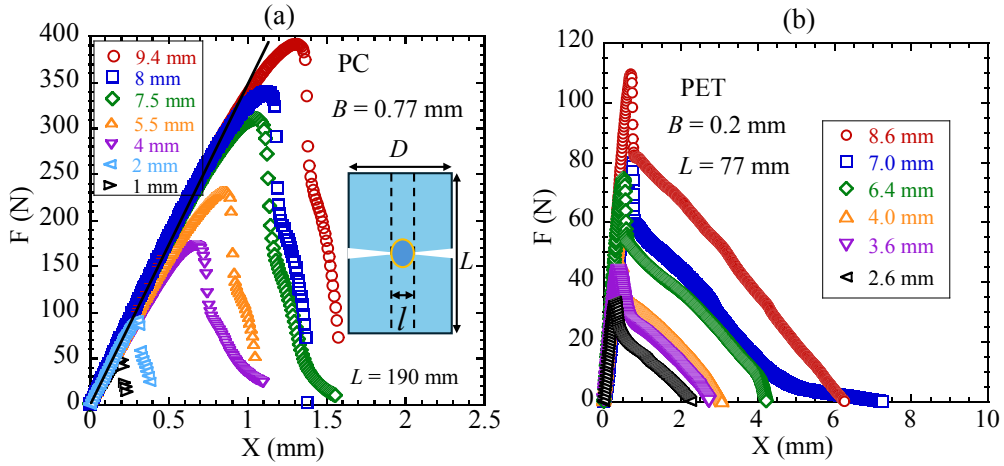

View Article Online
DOI: 10.1039/D6SM00148C

Figure 4 Mechanical responses of DENT specimens in terms of tensile force vs. displacement X for (a) PC (B = 0.77 mm) and (b) PET (B = 0.2 mm) at different ligament lengths. The inset (a) illustrates the DENT configuration.

3.3.2 Force-displacement linearity

According to Figure 4(a)-(b), the linearity between F and X holds nearly up to the force maximum. Thus, the linear scaling is observed throughout the full range of displacement including regimes where tip yielding (TY) and ligament necking (LN) take place. *Str*-POM measurements can quantify stress intensification at the notch tips, which are the two edges in DENT, in terms of the birefringence fringe order (N_{tip}) and identify the onset of tip yielding. Moreover, *str*-POM observations allow us to confirm the assertion that the strain field in the ligament is given by Eq. (2): At a common value of ε_{lig} or fixed "far-field" σ_{lig} the tip birefringence should be the same, independent of l. For example, reading from Figure 5(a) the first and sixth squares, at N_{tip} = 16, tip yielding emerges at F = 25 N (X = 0.094 mm) for l = 1 mm and F=230 N (X =0.64 mm) for l = 8 mm, corresponding to σ_{lig} = 40 MPa (l = 1 mm) and 34 MPa (l = 8 mm). This value of σ_{lig} is approximately half of the yield stress $\sigma_y \approx 70$ MPa, as if the stress intensification factor is around two, independent of ligament length.

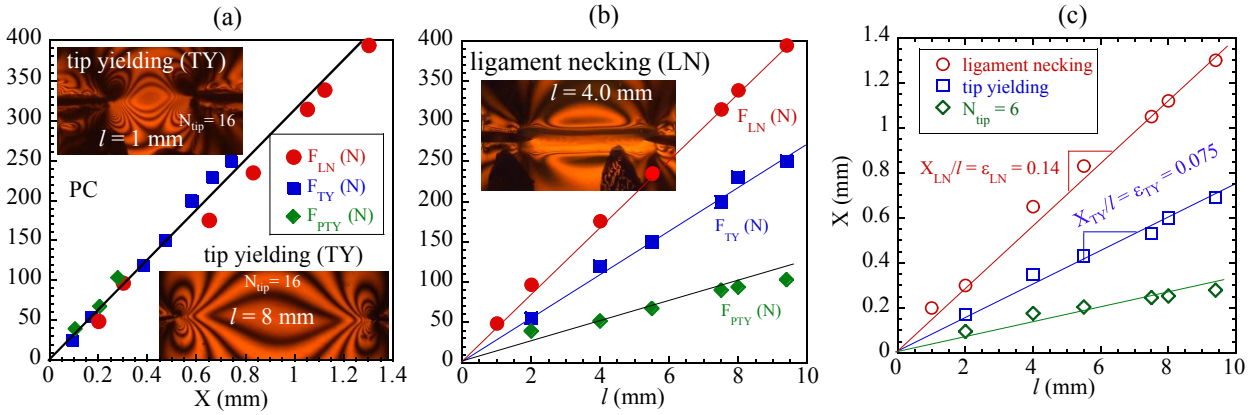

Figure 5 (a) Tensile force vs. displacement for all ligament lengths at three characteristic states: pre-tip-yielding (PTY, N_{tip} = 10), tip yielding (TY, N_{tip} = 16), and total ligament necking (LN) at the maximum force, where the two images show that the tip birefringence orders reach the same value of N_{tip} = 16. (b) Tensile forces at the three states, F_{PTY}, F_{TY}, and F_{LN}, plotted against ligament length l, showing linear scaling. (c) Linear relationship between displacement and ligament length to confirm that each of the three states involves a common effective strain $\varepsilon_{lig} = X/l$.

Figure 5(a) contains the two images of the birefringence pattern at tip yielding, along with relationship between force and displacement for all ligament lengths at pre-tip-yielding (PTY – N_{tip}=10), tip yielding (TY – N_{tip} = 16) and total ligament necking (LN) at the force maximum. The linearity in Eq. (3) also manifests in linear relationships between tensile force F_{PTY}, F_{TY} and F_{LN}

View Article Online
DOI: 10.1039/D6SM00148C

and ligament length l, as shown in Figure 5(b). Finally, a common strain ε_{lig} to produce these three special states among all specimens of different ligament length implies a third linearity, as shown in Figure 5(c).

Using the *str*-POM method, we explore the stress intensification in DENT to the tip stress to the remote load, which may be expressed in terms of the effective strain ε_{lig} given in Eq. (2). To convert birefringence order N to tensile strength, we first obtain the calibration, i.e., the stress-optical relation (SOR) in Figure 6(a). Here linearity breaks down as PC undergoes partial yielding. At the notch tips (edges of DENT), Figure 6(b) shows the tip birefringence linearly increases with the "far field" strain ε_{lig}. Given Eq. (1) and that linearity in SOR in Figure 6(a) is bounded by 40 MPa, the horizontal axis of Figure 6(b) is proportional to fringe order N so that Figure 6(b) shows $N_{tip} = 2N$, independent of l for the explored range 3 mm to 9.3 mm. In contrast, in SEN with notch length a *str*-POM observations of SEN revealed[7, 21] that at a common tip stress or birefringence the far-field stress $\sigma \sim a^{-1/2}$. It is remarkable that neither ligament length l nor tip curvature appears in the stress intensification in DENT. Converting to stress based on SOR in Figure 6(a), Figure 6(c) shows the stress intensification at the tip. Here the initial slope is two, i.e., the tip stress intensifies by a factor of two, and the nonlinear relationship between σ_{tip} and σ_{lig} arises from partial tip yielding.

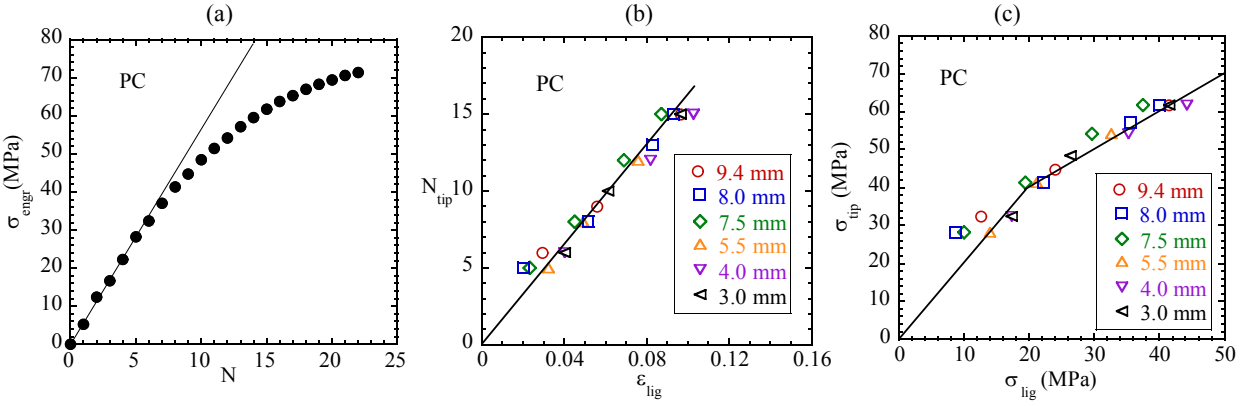

Figure 6 (a) Stress-optical relationship measured from unnotched PC. (b) Tip (edge) birefringence as a function of effective strain ε_{lig} of Eq. (2) for different ligament lengths. (c) Tip stress vs."far field load" σ_{lig}.

The scaling behavior of PC in DENT takes place within linear elasticity. Analyzing the DENT tests presented in Figure 4(b), we confirm that PET also displays the same linearities, as shown in Figure 7(a) and 7(b).

View Article Online
DOI: 10.1039/D6SM00148C

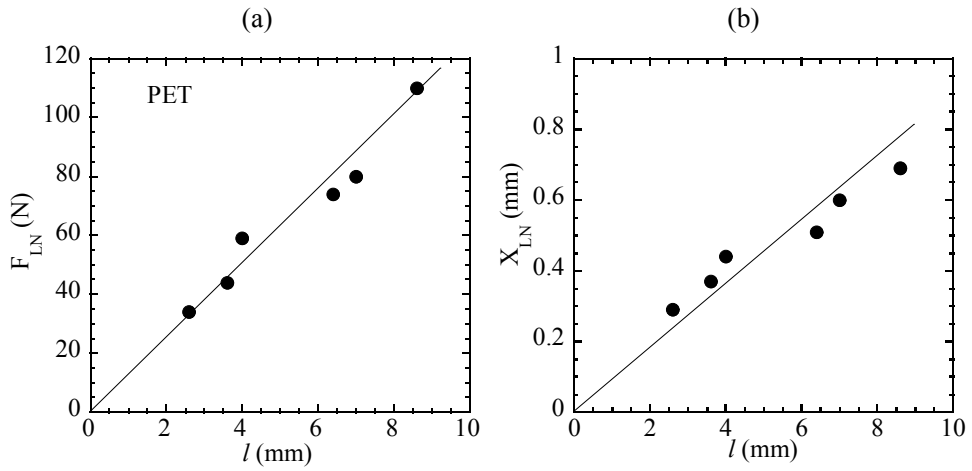

Figure 7 Tensile force at ligament necking F_{NL} vs. ligament length l. (c) Linear relationship between displacement and ligament length to confirm that ligament necking involves a common effective strain $\varepsilon_{lig} = X/l$.

3.4 Brittle polystyrene in DENT: thickness effect

To explore the condition for Eq. (2) and Eq. (3) to hold in DENT for linear elastic materials, we examine a brittle polystyrene that undergoes fracture at room temperature within linear elasticity. The chain network breaks down via chain pullout before yielding.[22-24] In other words, at room temperature brittle PS is incapable of undergoing plastic deformation. By changing thickness B from 0.55 to 1.5 mm, the scaling behavior of F ~ X, described in Eq. (3) and seen from Figures 4(a)-(b), from which Figures 5(a)-(c) and 7(a)-(b) arise, disappears. Figure 8(a) is replaced by Figure 8(b), which shows higher force responses for higher ligament length. Thus, the effective strain defined in Eq. (2) appears to be valid only when specimens are thin enough, where perhaps plane-stress deformation prevails. At the present time, to the best of our knowledge, we are unaware of any theoretical calculation that demonstrates such a thickness effect or derives Eq. (1) to Eq. (2).

At B = 0.55 mm, PS in DENT with smaller l shows the same level of mechanical resistance (in terms of tensile force F) against displacement X, like PC and PET. However, since PS can be expected to fracture at the same local tip stress, Figure 8(c) explicitly confirms that fracture occurs at a common level of σ_{lig}. In other words, specimens with larger l are stronger and more strain tolerant, as indicated in Figure 8(a). As far as fracture conditions are concerned, the thickness effect is unremarkable, as shown by the comparison between circles and squares in Figure 8(c). In other words, PS in DENT experiences brittle fracture like fracture observed with notch-free specimen. On the other hand, $\sigma_{lig(fract)}$ is well defined and shows relatively small range of uncertainty. Thus, for flaw-tolerant brittle materials including PS, DENT is a rather interesting protocol for fracture characterization. Here we can apply the conclusion established in Figure 8(c), i.e., $\sigma_{tip} = 2\sigma_{lig}$, to estimate fracture stress of PS as $\sigma_b = 2\sigma_{lig(fract)}$, i.e., ca. 50 MPa, which is indeed a typical value for PS, as shown in Figure SI.1 in Supporting Information (SI).

View Article Online
DOI: 10.1039/D6SM00148C

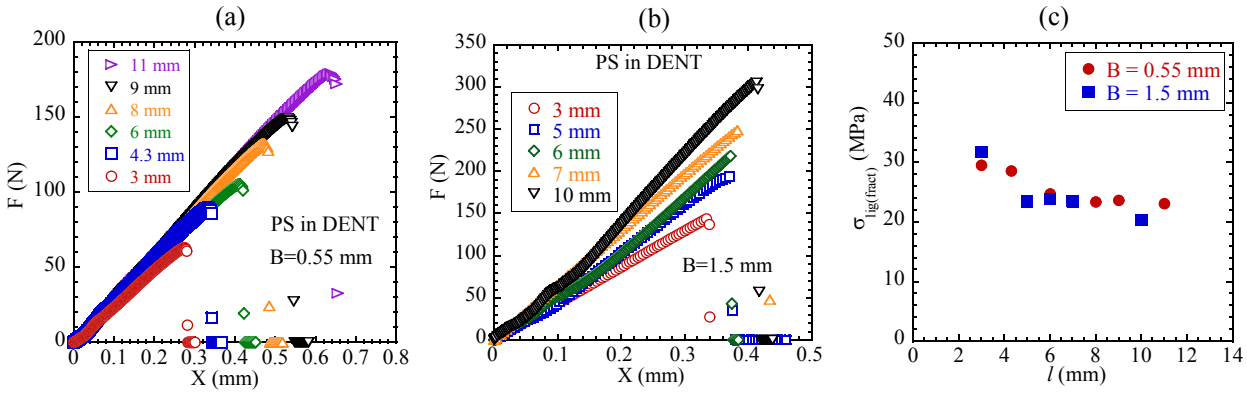

Figure 8 (a) Force vs. displacement curves for (a) thin PS (B = 0.55 mm) and (b) thick PS (B = 1.5 mm) specimens with various ligament lengths l. (c) Nominal stress σ_{lig} defined by Eq. (1) at brittle fracture as a function of ligament length for both thicknesses.

3.5 Elastomer in DENT

The linear relation of Eq. (3) may occur for any linear elastic materials if DENT specimens are thin enough. We examine one more type of solid that may exhibit the scaling behavior of Eq. (3). Highly-crosslinked BR1phr follows linear elastic fracture mechanics and develops fast crack growth in a narrow range of applied far-field stress. When it is thin enough, e.g., with B = 0.7 mm, the force resistance is like that of PS as shown in Figure 9(a). In contrast, BR1phr with B = 1.5 mm behaves like the thicker PS because Figure 9(b) resembles Figure 8(b).

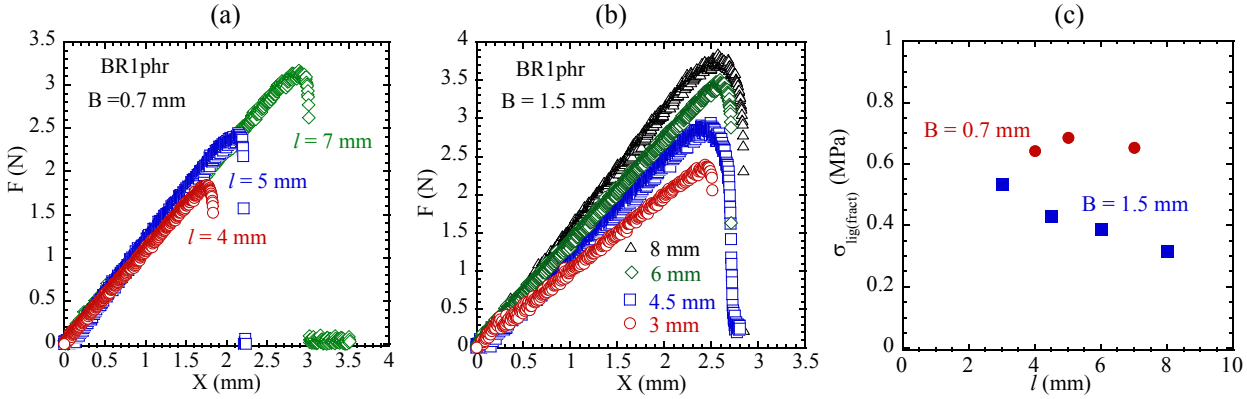

Figure 9 Force vs. displacement curves for DENT specimens of crosslinked polybutadiene BR1phr for (a) thickness B = 0.7 mm and (b) B =1.5 mm at different ligament lengths. (c) Nominal ligament stress at fracture as a function of l, showing little dependence at B = 0.7 mm.

Unlike PS, with sufficient birefringence and linear SOR for BR1phr, we can further illustrate and confirm how stress intensification at the edges of DENT takes place, driven by the far-field load. Specifically, like Figure 6(b), Figure 10(a) shows that the birefringence order N_{tip} at the tips increases linearly with the effective far-field stress σ_{lig}. In contrast, with thicker BR =

View Article Online
DOI: 10.1039/D6SM00148C

1.5 mm, Figure 10(b) shows that the tip birefringence becomes linearly dependent on F instead of $F/l \sim \sigma_{lig}$. The birefringence images in Figure 10(a)-(b) display the deformation of BR1phr specimens under a far-field load of 1.5 N. For the thin sample (B = 0.7 mm), higher tip birefringence shows up for l = 4 mm than for l = 7 mm because it depends on F/l rather than on F alone. In contrast, for the thick sample the same tip birefringence order appears for l = 3 mm and l = 9 mm, indicating that the tensile force F dictates the tip birefringence regardless of ligament length.

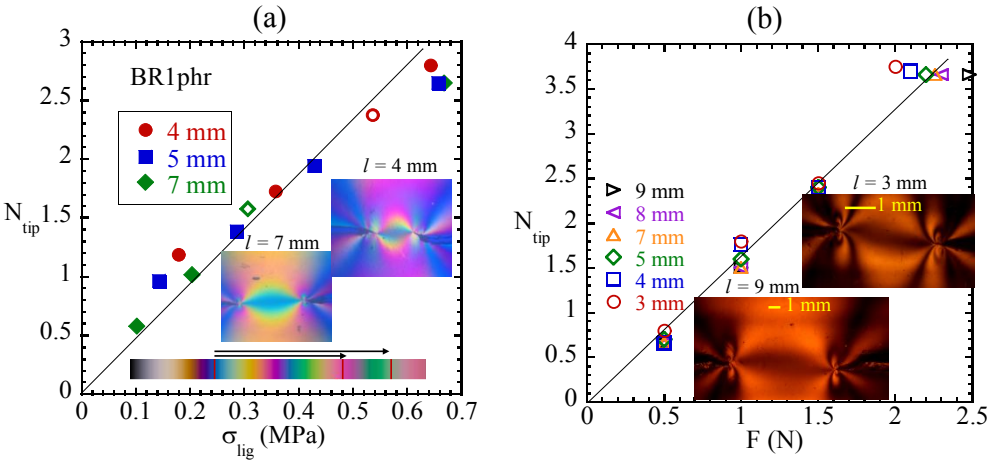

Figure 10. Evolution of the local notch-tip birefringence, N_{tip}, as a function of σ_{lig} for polybutadiene (BR) specimens with thickness (a) B = 0.7 mm and (b) B = 1.5 mm. Images show birefringence pattern at a fixed load of F = 1.5 N, corresponding to the two open symbols in (a).

3.6 Essential work from DENT

For ductile materials that can undergo considerable plastic deformation, Cotterell and Reddel (CR)[25] first proposed to investigate their mechanical responses in DENT configuration, provided the ligament length l is smaller than twice the maximum plastic zone size r_p^*. In this limit, along with $l > 5B$, CR envisioned that the total mechanical work W needed to drive crack growth beyond tip yielding until final macroscopic separation should comprise both a linear and quadratic terms. The dominant part of W should scale quadratically with l since plastic deformation may occur in a region whose volume is quadratic in l, i.e.,

$$W = w_e l B + w_p B l^2, \text{ where } l < 2r_p^* \text{ and } l > 5B, \quad (4)$$

so that

$$w_f = W/lB = w_e + w_p l. \quad (5)$$

However, we showed that linear-elastic materials such as PS and BR1phr examined in the preceding Sections 3.4 and 3.5 also indicate a quadratic dependent of W on l^2. In other words, when specimens in DENT are sufficient thin for Eq. (2) and Eq. (3) to be valid, W for fracture also

View Article Online
DOI: 10.1039/D6SM00148C

follows Eq. (4) or Eq. (5) in absence of plasticity. For example, according to Figures 8(a) and 9(a), $W = FX = l^2(F/l)(X/l) \sim l^2$ because F (~X) and X both linearly increases with l until fracture. Figures 11(a)-(b) show w_f vs. l with clearly defined intercept at $l = 0$ as w_e. The value for w_e is consistent with reported[19] toughness G_c for PS, however, $w_e \sim 0.5$ kJ/m^2 is more than twice that of $G_c = 0.21$ kJ/m^2, which is estimated from pure shear measurements using Rivlin-Thomas formula,[15] as shown in Supporting Information Figure SI2.

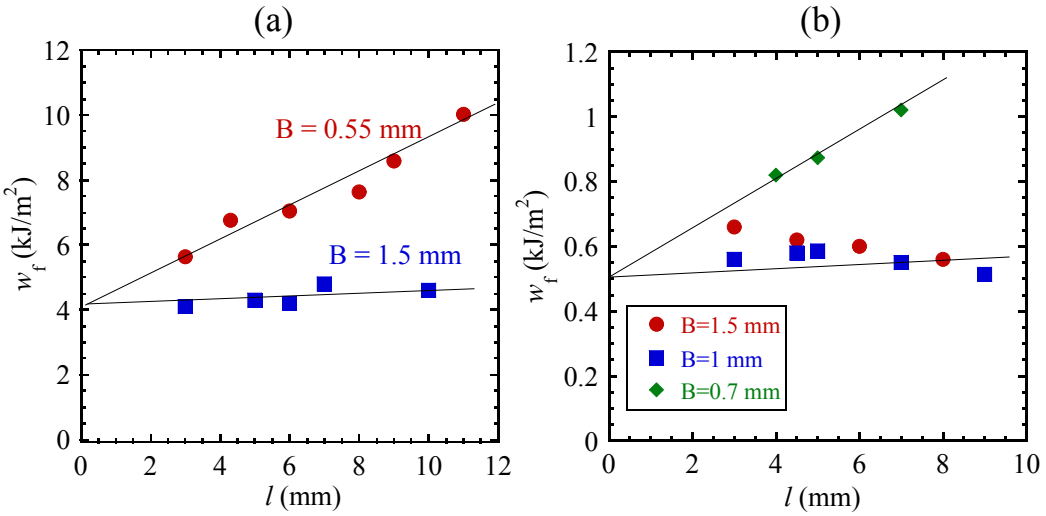

Figure 11 Specific work of fracture w_f, plotted as a function of ligament length l, for (a) PS of thickness B = 0.55 and 1.5 mm and (b) BR1phr of thickness B = 0.7, 1 and 1.5 mm.

Finally, because of the scaling characteristics displayed in Eq. (2) and Eq. (3), the essential work w_e can be evaluated from Figures 4(a)-(b) for PC and PET, either up to the force maximum or by integrating over the "tails" associated with ligament necking, which is massive for PET and little for PC, and negligible for BR1phr and non-existent for PS. Figures 12(a)-(b) show $w_e = 5$ kJ/m^2 for PC and 20 kJ/m^2 for PET, which is consistent with the literature.[26]

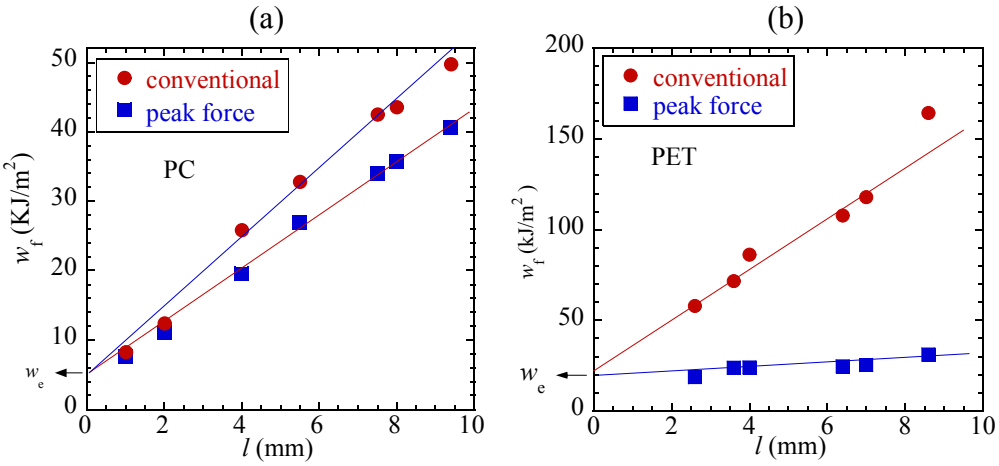

View Article Online
DOI: 10.1039/D6SM00148C

Figure 12 Specific work of fracture, w_f, plotted versus ligament length l, based on either total area under force vs. displacement curves (conventional) or area up to the maximum (peak force) for (a) PC and (b) PET.

4. Discussion

The *str*-POM method has allowed us to describe what happens at notch tip and confirm the existence of SSZ that Creager-Paris solution[14] predicted in the linear elasticity limit. In other words, C-P solution predicts the existence of SSZ and elucidates the origin of SSZ that we observed in PS and BR. Since SSZ emerges in these brittle polymers as well as ductile PC and PET below the tip yielding threshold, it is not the plastic zone that Irwin proposed for metals. The absence of notch tip yielding below a finite far-field load conversely reveals that notch tips are only of finite sharpness. The size of SSZ reveals the level of tip blunting in these materials. Although existence of a damage or process zone[5] has been suggested initially[27-30] for metals, the concept has been adopted[4] for polymers including plastics and elastomers. One of the large aims of the present study is precisely to raise a question about the past treatment of polymer fracture. Our observations suggest the SSZ emerges before fracture and thus does not coincide with the concept of damage zone. While emergence of SSZ supports the C-P description of tip stress, beyond linear elasticity and finite spatial resolution of the *str*-POM method we cannot be certain that only elastic SSZ is present at finite loads. On the other hand, there is little indication that PC, PET and well-crosslinked BR cannot be regarded to only show linear-elastic responses before tip yielding for PC and PET and fracture for BR.

In elastomers that undergo purely elastic stretching at temperatures well above the glassy transition temperature T_g, there is neither plastic process nor viscous dissipation at crack tip. For example, BR has $T_g = -100$ °C and does not develop a process zone. In the case of fracture of thermoplastic elastomers,[31] more complicated processes may take place at notch tip. Further discussion is beyond the scope of the present study.

5. Conclusions

We have employed the *str*-POM method to investigate several important questions in the field of polymer fracture. The access to tip stress based on photoelastic effects shows that no sizable plastic zone exists in ductile PET below a critical load (cf. Fig. 2(a)). Thanks to *str*-POM observations, we have generalized Griffith scaling law and confirmed the Creager-Paris solution using PC and PET below tip yielding: Stress intensity factor K prescribes the tip stress so that $\sigma \sim a^{-1/2}$ produces a common tip stress (cf. Fig. 1(c) and Fig. 2(e)) prior to tip yielding and plasticity at notch tip. For elastomers in the linear elastic limit, there exists a finite stress saturation zone (e.g., $r_{ss} \geq 40$ μm, cf. Fig. 3(b)) before fracture so that energy release rate G involves release of stored elastic energy over a spatial region of size r_{ss}, far greater than a monolayer thickness. This observation can explain why G reaches a much higher level than G_0.

So far, single-edge notch (SEN) has been a dominant configuration for fracture mechanics investigation of various brittle materials including plastics and elastomers. Ductile materials are not subject to Griffith's account and may be characterized by resistance curves. To quantify energy

View Article Online
DOI: 10.1039/D6SM00148C

involved in ductile fracture, double-edge-notch tension (DENT) is widely used to extract the essential work w_e as a quantity "equivalent" to Griffith's toughness. Application of *str*-POM allows us to elucidate how stress builds up at the tip of double edges in DENT and produce insight into the origin of w_e. We found for both plastics (ductile and brittle) and elastomers (well-crosslinked) that in the limit of linear elasticity and under the condition of plane stress (or for specimens sufficiently thin) stress intensification at notch tip is independent of ligament length (cf. Fig. 8(c) and Fig. 9(c)) and depends only on the effective strain, which is displacement X normalized by ligament length l (cf. Fig. 6(b) and Fig. 10(a)). Thus, surprisingly, prior to failure and within the explored range of ligament length l, the tensile force arising from drawing is independent l (cf. Fig. 4(a)-(b), Fig. 8(a) and Fig. 9(a)). Moreover, this peculiar scaling, validated using linear-elastic brittle solids such as PS and highly-crosslinked BR (cf. Fig. 12(a)-(b)), necessarily produces a term in the total mechanical work that is quadratic in l although no plastic deformation is involved.

Acknowledgments

This work is supported, in part, by the Polymers program at the US National Science Foundation through Special Creativity Extension of grant DMR-2210184.

Credit author statement

Asal Y Siavoshani: Quantitative birefringence measurements, Data curation. Formal Analysis, Validation, Writing – experimental section. Zehao Fan: Curation of data in Figure 3. Shi-Qing Wang: Supervision, Conceptualization, Methodology, Formal Analysis, Validation._Writing – drafting, reviewing and editing.

View Article Online
DOI: 10.1039/D6SM00148C

References

1. J. Williams, *Polymer Engineering & Science*, 1977, **17**, 144-149.
2. C. B. Bucknall, *Toughened plastics*, Springer, **1977**.
3. I. M. Ward and J. Sweeney, *Mechanical properties of solid polymers, 3rd*, John Wiley & Sons, Ltd., Chichester, UK, **2012**.
4. A. J. Kinloch and R. J. Young, *Fracture behaviour of polymers*, Springer Science & Business Media, **2013**.
5. C. Creton and M. Ciccotti, *Rep. Prog. Phys.*, 2016, **79**, 046601.
6. C. Creton, *Macromolecules*, 2017, **50**, 8297-8316.
7. T. Smith, C. Gupta, Z. Fan, G. J. Brust, R. Vogelsong, C. Carr and S.-Q. Wang, *Extreme Mechanics Letters*, 2022, **56**, 101819.
8. C. Gupta, A. Siavoshani and S.-Q. Wang, *Polymer*, 2025, **337**, 128929.
9. S.-Q. Wang, Z. Fan, C. Gupta, A. Siavoshani and T. Smith, *Macromolecules*, 2024, **57**, 3875-3900.
10. S.-Q. Wang, Z. Fan, A. Siavoshani, M.-c. Wang and J. Wang, *Extreme Mechanics Letters*, 2024, **74**, 102277.
11. A. Y. Siavoshani, M.-C. Wang, C. Liang, A. Jaisingh, J. Wang, C. Wang and S.-Q. Wang, *Macromolecules*, 2026, **59**, 2885.
12. S.-Q. Wang, *Polymer Physics: Ductility, Fracture, and Adhesion*, Wiley, 2026.
13. C. E. Inglis, *Trans Inst Naval Archit*, 1913, **55**, 219-241.
14. M. Creager and P. C. Paris, *International journal of fracture mechanics*, 1967, **3**, 247-252.
15. Z. Fan and S.-Q. Wang, *Extreme Mechanics Letters*, 2023, **61**, 101986.
16. S.-Q. Wang and Z. Fan, *Rubber Chem. Technol.*, 2023, **96**, 530-550.
17. T. L. Smith and P. J. Stedry, *J. Appl. Phys.*, 1960, **31**, 1892-1898.
18. J. Berry, *J. Polym. Sci.*, 1961, **50**, 107-115.
19. J. Berry, *J. Polym. Sci.*, 1961, **50**, 313-321.
20. T. L. Anderson, *Fracture mechanics: fundamentals and applications*, CRC press, **2005**.
21. A. Siavoshani and S.-Q. Wang, *Macromolecules*, 2026, to appear soon.
22. S.-Q. Wang, S. Cheng, P. Lin and X. Li, *J. Chem. Phys.*, 2014, **141**, 094905.
23. M. Razavi, S. Cheng, D. Huang, S. Zhang and S.-Q. Wang, *Polymer*, 2020, **197**, 122445.
24. A. Siavoshani and S.-Q. Wang, *Macromolecules*, 2026, **59**, 279.
25. B. Cotterell and J. Reddel, *Int J Fract*, 1977, **13**, 267-277.
26. W. Chan and J. Williams, *Polymer*, 1994, **35**, 1666-1672.
27. G. Irwin, *Proceedings of the 7th Sagamore Ordnanc Materials Conference, Syracuse University*, 1961, 63-78.
28. G. I. Barenblatt, *Journal of applied mathematics and mechanics*, 1959, **23**, 622-636.
29. D. S. Dugdale, *Journal of the Mechanics and Physics of Solids*, 1960, **8**, 100-104.
30. B. A. Bilby, A. H. Cottrell and K. Swinden, *Proceedings of the Royal Society of London. Series A. Mathematical and Physical Sciences*, 1963, **272**, 304-314.
31. S. Sbrescia, J. Ju, C. Creton, T. Engels and M. Seitz, *Soft Matter*, 2023, **19**, 5127-5141.

View Article Online
DOI: 10.1039/D6SM00148C

The data supporting this article have been included as part of the Supplementary Information.